Perturbative nonlinear feedback forces for optical levitation experiments

Oscar Kremer,[1] Daniel Tandeitnik,[2] Rafael Mufato,[2] Igor Califrer,[2] Breno Calderoni,[2] Felipe Calliari,[1] Bruno Melo,[3] Guilherme Temporão,[1] and Thiago Guerreiro[2,*]

[1]*Center for Telecommunications Studies, Pontifical Catholic University of Rio de Janeiro, 22451-900 Rio de Janeiro, Brazil*

[2]*Department of Physics, Pontifical Catholic University of Rio de Janeiro, 22451-900 Rio de Janeiro, Brazil*

[3]*Nanophotonic Systems Laboratory, Department of Mechanical and Process Engineering, ETH Zürich, 8092 Zürich, Switzerland*

(Received 29 September 2023; accepted 23 January 2024; published 20 February 2024)

Feedback control can be used to generate well-determined nonlinear effective potentials in an optical trap, a goal whose applications may range from nonequilibrium thermodynamics to the generation of non-Gaussian states of mechanical motion. Here, we investigate the action of an effective feedback-generated quartic potential on a levitated nanoparticle within the perturbation regime. The effects of feedback delay are discussed and predictions from the perturbation theory of a Brownian particle subjected to a quartic anharmonicity are experimentally verified.

DOI: 10.1103/PhysRevA.109.023521

I. INTRODUCTION

Optical levitation of nanoparticles provides a robust setup for both fundamental and applied physics [1,2], from classical stochastic thermodynamics [3–6] to mesoscopic quantum science [7–9]. In the typical levitated optomechanics experiment, a dielectric particle is trapped in a tightly focused Gaussian beam providing, to leading-order approximation, a confining harmonic potential [10,11]. The particle undergoes Brownian motion due to interaction with its surrounding medium and measurements of its position correlation functions, notably the autocorrelation and the associated power spectrum, allows for the characterization of the trap's parameters [11,12].

While the harmonic approximation is commonly employed in optical trapping, the ability to engineer potential landscapes beyond the quadratic approximation is central to optomechanics. Nonlinear force landscapes are a valuable resource to nonequilibrium Brownian machines [13,14], the preparation of nonclassical and non-Gaussian quantum states [15], and matter-wave interference experiments [16], to mention just a few examples. Nonlinear potential landscapes also appear in structured light optical tweezers [17], as in double-well landscapes [18–21], structured light beams with pattern revivals [22], cylindrical vector beams [23], and dark focus traps [24,25].

In these nonlinear potential landscapes, to which we refer here as *nonlinear optical tweezers*, a quantitative statistical description of the stochastic particle motion is significantly more complicated as it involves nonlinear stochastic differential equations. To make quantitative predictions regarding the statistical correlators of the trapped particle's motion, we can, however, resort to perturbation theory [26].

A perturbative method for nonlinear optical tweezers has been developed in [27], wherein it is possible to compute corrections to the statistical moments of particle motion, in particular the position power spectrum. The purpose of the present work is to experimentally validate these methods. In standard Gaussian optical tweezers, the ratio between linear and nonlinear spring constants cannot be varied independently, given that both scale linearly with the trapping power [28,29]. Thus, we turn to effective feedback potential landscapes to implement nonlinear position-dependent forces upon a levitated nanosphere. We implement the nonlinearity via electric feedback and characterize its effects on the particle motion.

This paper is organized as follows. In the next section, we briefly review the perturbation theory for computing corrections to the correlation functions of a trapped particle under the influence of a nonlinear force, and generalize it to include the effect of delayed forces. Since we deal with artificial electric feedback potentials relying on measurements and processing of the trapped particle's position, they imply an inherent delay to the nonlinear force and therefore accounting for the effects of this delay is essential to validating the methods of [27]. We then describe the experimental setup used to generate nonlinear potential landscapes through electric feedback on the particle and numerically compute the effects of delay, showing that within the range of parameters employed in our experiment, they are negligible. We implement a cubic force (quartic potential) on the particle and, finally, verify the perturbation theory by comparing the predicted center frequency of the position power spectral density with experimental results. We conclude with a brief discussion of the applications of artificial nonlinear forces to levitated optomechanics experiments.

II. THEORY

A. Formulation of the perturbation theory

We model the stochastic motion of a particle in a fluid at thermal equilibrium at temperature T_{eff} and under a force field

*barbosa@puc-rio.br

$\vec{F}(\vec{r})$ using the Langevin equation,

$$\ddot{\vec{r}}(t) = -\Gamma_m \dot{\vec{r}}(t) + \vec{F}(\vec{r}(t))/m + \sqrt{C}\vec{\eta}(t), \tag{1}$$

where m is the particle's mass, $\Gamma_m = \Gamma/m$, $C = 2\Gamma k_B T_{\text{eff}}/m^2$ with Γ the drag coefficient, and $\vec{\eta}(t)$ is isotropic Gaussian white noise, whose components satisfy

$$\mathbb{E}[\eta_i(t)\eta_j(t')] = \delta_{ij}\delta(t-t'). \tag{2}$$

Concentrating in the motion along the longitudinal z direction, Eq. (1) reduces to a one-dimensional Langevin equation,

$$\ddot{z}(t) = -\Gamma_m \dot{z}(t) + F_z(z(t))/m + \sqrt{C}\eta(t). \tag{3}$$

For an approximately linear trapping force perturbed by nonlinear corrections, the steady-state position autocorrelation $A(t) \equiv \mathbb{E}[z(t)z(0)]$ can be perturbatively approximated. We next summarize the perturbation theory outlined in [27] and used throughout this work.

Consider the force acting on the particle,

$$F_z(z) = -m\omega_0^2 z - G_{\text{fb}} z^3, \tag{4}$$

where the first term accounts for an optical trap with resonance frequency ω_0 and the second term is a small nonlinear correction, which in the experiment originates from a feedback force on the particle proportional to the *feedback gain* G_{fb} times a nonlinear function of the particle's position. We define the Green's function,

$$G(t) = \frac{\sin(\Omega t)}{\Omega}\, \exp\left(-\frac{\Gamma_m t}{2}\right) H(t), \tag{5}$$

where $\Omega = \sqrt{\omega_0^2 - \Gamma_m^2/4}$ and $H(t)$ is the Heaviside step function with $H(t) = 1$ for $t > 0$ and $H(t) = 0$ for $t \leqslant 0$. We introduce the auxiliary variable (also referred to as the response paths) $\tilde{z}(s)$ and define the Wick sum bracket $\langle(\cdot)\rangle_0$:

$$\langle z(t_1)\cdots z(t_n)\tilde{z}(s_1)\cdots\tilde{z}(s_m)\rangle_0 = \delta_{nm}\sum_{\sigma}\prod_{j=1}^{n} G(t_j - s_{\sigma(j)}), \tag{6}$$

where the sum goes over all permutations σ of indexes $\{1,\ldots,n\}$. The response variables $\tilde{z}(s)$ can be understood as auxiliary integration variables in a stochastic path integral defining the perturbation theory expansion; we refer to [26,27] for details on stochastic perturbation methods. Note that the second-order correlator is given by the Green's function, $\langle z(t)\tilde{z}(s)\rangle_0 = G(t-s)$. The perturbation theory is summarized by the expression for the position autocorrelation function,

$$\begin{aligned} A(t) &\equiv \mathbb{E}[z(t)z(0)] \\ &= \left\langle z(t)z(0)e^{\frac{C}{2}\int\tilde{z}^2(s)ds}e^{\frac{G_{\text{fb}}}{m}\int\tilde{z}^3(t')z(t')dt'}\right\rangle_0, \end{aligned} \tag{7}$$

where the right-hand side is defined by expanding both exponentials inside the brackets as a power series in C and in G_{fb}/m and interchanging summations and integrations by applying the Wick bracket $\langle(\cdot)\rangle_0$. Note that only brackets with an equal number of z and $\tilde{z}$ variables are nonvanishing [26,27].

The first nonvanishing term in the expansion of Eq. (7) is

$$\frac{C}{2}\int\langle z(t)z(0)\tilde{z}^2(s)\rangle_0\, ds = C\int G(t-s)G(-s)ds, \tag{8}$$

which gives the autocorrelation for the case of a linear force $F_z(x) = -m\omega_0^2 z$,

$$A(t)_{(G_{\text{fb}}=0)} = \frac{Ce^{-\Gamma_m|t|/2}(2\Omega\cos\Omega|t| + \Gamma_m\sin\Omega|t|)}{\Gamma_m\Omega\left(\Gamma_m^2 + 4\Omega^2\right)}. \tag{9}$$

The leading-order correction in the feedback gain reads

$$\begin{aligned} &\Delta A(t) \\ &\quad\equiv \frac{C^2 G_{\text{fb}}}{8m}\int\langle\tilde{z}^2(s_1)\tilde{z}^2(s_2)\tilde{z}(t_1)z^3(t_1)z(t)z(0)\rangle_0\, ds_1 ds_2 dt_1. \end{aligned} \tag{10}$$

Expanding the brackets using (6) would produce a sum with $5! = 120$ terms, but many of these vanish since $\langle\tilde{z}(t_1)z(t_1)\rangle = G(0) = 0$. Moreover, by symmetry of the integration variables s_1 and s_2, the contribution to the integral of the nonvanishing terms is equal to the contribution of $G(t-t_1)G(-s_1)G(t_1-s_1)G^2(t_1-s_2)$ or $G(-t_1)G(t-s_1)G(t_1-s_1)G^2(t_1-s_2)$. Therefore, the integral in (10) is computed by integrating these two terms over t_1, s_1, s_2 and multiplying both integrals by a multiplicity factor $2^3(3!) = 48$. We note that a diagrammatic expansion can be employed to organize nonvanishing terms in the Wick sum; for more details, we refer to [27].

From the autocorrelation function perturbation ΔA, we can obtain the correction in the power spectral density (PSD) of the particle motion by taking the Fourier transform [27],

$$\Delta S = \frac{3G_{\text{fb}}C^2}{\Gamma_m\omega_0^2}\frac{\omega^2-\omega_0^2}{\left[\Gamma_m^2\omega^2 + \left(\omega^2-\omega_0^2\right)^2\right]^2}. \tag{11}$$

The PSD of the motion of a particle with unperturbed resonance frequency ω_0 subject to a frequency shift $\Delta\Omega$ can be expanded to first order as

$$\begin{aligned} &\frac{C}{\Gamma_m^2\omega^2 + [\omega^2 - (\omega_0+\Delta\Omega)^2]^2} \\ &\quad\approx \frac{C}{\Gamma_m^2\omega^2 + \left(\omega^2-\omega_0^2\right)^2} \\ &\qquad + 4C\omega_0\Delta\Omega\frac{\omega^2-\omega_0^2}{\left[\Gamma_m^2\omega^2 + \left(\omega^2-\omega_0^2\right)^2\right]^2}. \end{aligned} \tag{12}$$

Comparing the first-order correction in Eq. (12) with the correction in Eq. (11), we conclude that the nonlinearity causes a frequency shift given by

$$\frac{\Delta\Omega}{2\pi} = \frac{3k_bT_{\text{eff}}}{4\pi m^2\omega_0^3}G_{\text{fb}} \equiv \kappa G_{\text{fb}}. \tag{13}$$

We see that effectively, the nonlinear perturbation manifests as a shift in the PSD central frequency scaling linearly with the feedback gain G_{fb} and with a slope given by the constant κ. This is valid for small G_{fb},

$$G_{\text{fb}} \ll \frac{m^2\omega_0^4}{2k_bT_{\text{eff}}}. \tag{14}$$

The right-hand side of (14) can be used to delimit the validity region of perturbation theory. The shift $\Delta\Omega$ in the central frequency of the PSD is the experimental signature which we use as an indicator of the effect of nonlinear perturbations. It

is worth noticing that the shift described by (13) also includes intrinsic nonlinearities of the tweezer, which arise due to anharmonicities of the trapping potential [28]. Note, however, that only relative shifts to the original resonance frequency (with the cubic feedback off, but in the presence of the intrinsic nonlinearities) are measured. Thus, our experiment is not sensitive to the intrinsic anharmonicities of the trap, but only to those affected by the cubic feedback.

B. Delayed nonlinearities

Besides nonlinear force perturbations, we will be interested in delayed forces. Artificially produced feedback forces will naturally be subject to electronic delay. Accounting for the effects of such delays in perturbation theory allows us to understand the limits of validity of Eq. (7) for modeling the artificial feedback forces. More broadly, understanding the role of delays might also enable the study of perturbative nonlinear non-Markovian stochastic dynamics [30].

We consider the generalized Langevin equation,

$$\ddot{z}(t) = -\Gamma_m \dot{z}(t) - \omega_0^2 z(t) - \frac{G_{\rm fb}}{m} z^3(t-\tau) + \sqrt{C}\,\eta(t), \quad (15)$$

where $\tau > 0$ is a fixed (constant) time delay. Note the delayed position can be written in terms of a memory kernel,

$$z(t-\tau) = \int z(s) K(t-s)\, ds, \quad (16)$$

where

$$K(t-s) = \delta(t-\tau-s). \quad (17)$$

The perturbation expansion for $\tau = 0$ [Eq. (7)] can then be generalized to

$$\begin{aligned} A(t,\tau) &\equiv \mathbb{E}[z(t)z(0)] \\ &= \left\langle z(t)z(0) e^{\frac{C}{2}\int \ddot{z}^2(s)ds} e^{\frac{G_{\rm fb}}{m}\int \ddot{z}(t')z^3(t'-\tau)dt'} \right\rangle_0. \end{aligned} \quad (18)$$

Expanding the exponentials in power series and using the Wick sum as defined in (6), the leading correction to the autocorrelation function (9) is given by the following integrals:

$$\begin{aligned} \Delta A(t,\tau) \propto & \int G(t-t_1)G(-s_1)G(t_1-s_1-\tau) \\ & \times G^2(t_1-s_2-\tau)dt_1 ds_1 ds_2 \\ & + \int G(-t_1)G(t-s_1)G(t_1-s_1-\tau) \\ & \times G^2(t_1-s_2-\tau)dt_1 ds_1 ds_2. \end{aligned} \quad (19)$$

We note that both integrals are multiplied by the constant $3G_{\rm fb}C^2/m$, which we omit to avoid cluttering the notation. Evaluating the integrals leads to the corrected autocorrelation function to first order in the perturbation,

$$\begin{aligned} A(t,\tau) = & \frac{Ce^{-\Gamma_m|t|/2}(2\Omega\cos\Omega|t| + \Gamma_m \sin\Omega|t|)}{\Gamma_m\Omega\left(\Gamma_m^2 + 4\Omega^2\right)} + \frac{3C^2 G_{\rm fb} e^{-\Gamma_m|t|/2}}{64m\Gamma_m^3\Omega^4\omega_0^6}\Big(e^{\Gamma_m\tau/2}\left[8\Gamma_m\Omega^4 - 4\omega_0^2\Gamma_m^2\Omega^2(|t|-\tau)\right]\cos[\Omega(|t|-\tau)] \\ & + e^{\Gamma_m\tau/2}\left[8\Gamma_m\Omega^3\omega_0^2(|t|-\tau) + 8\Omega^5 + 4\Gamma_m^2\omega_0^2\Omega + 6\Gamma_m^2\Omega^3\right]\sin[\Omega(|t|-\tau)] \\ & + e^{-\Gamma_m\tau/2}\left\{\Omega^2\left(2\Gamma_m^2\Omega - 8\Omega^3\right)\sin[\Omega(|t|+\tau)] + 8\Gamma_m\Omega^4\cos[\Omega(|t|+\tau)]\right\}\Big) + O\left(G_{\rm fb}^2, C^3\right). \end{aligned} \quad (20)$$

The quantity $A(0,\tau)$ can be experimentally obtained from the area under the PSD of the particle's motion, which in turn can be related to the mean occupation number of the mechanical modes. In what follows, we use these expressions to account for the effects of delay in the artificially generated nonlinear forces and to show that perturbation theory in the absence of delay provides a good approximation to current experiments.

III. EXPERIMENT

A simplified schematic of the experimental setup is shown in Fig. 1. A CW laser at 780 nm (Toptica DL-Pro) is amplified using a tapered amplifier (Toptica BoosTa) producing up to 1.5 W at the output of a single-mode fiber, yielding a high-quality Gaussian beam. The beam is expanded to overfill an aspheric lens of numerical aperture NA = 0.77 (LightPath 355330) mounted inside a vacuum chamber, which provides a tightly focused Gaussian beam to form the optical trap. A solution of silica spheres of diameter $2R = 143$ nm (MicroParticles GmbH) is monodispersed in ethanol and delivered into the optical trap using a nebulizer. Once a single particle is trapped, the pressure in the chamber is reduced to 10 mbar. The trapped particle's axial center-of-mass (COM) motion, $z(t)$, is recorded by collecting forward scattered light with an aspheric lens of numerical aperture NA = 0.50, and directing it to a photodiode (Thorlabs PDA100A2), generating an electric signal proportional to $z(t)$.

The signal from the detector is sent to a wide bandpass filter, amplified, and then input into an field-programmable gate array (FPGA). The FPGA introduces a tunable delay, raises the signal to the third power, and multiplies it by a tunable gain. The output signal is then amplified once again and applied to the mount of the trapping lens, producing a voltage difference with respect to the mount of the collection lens, which is grounded. This generates an electric force at the particle position given by $G_{\rm fb}z^3(t-\tau)$, where τ is the total delay introduced by the electronics and $G_{\rm fb}$ is the overall feedback gain. For more details on the generated electric field and electronics, see Appendices A and B.

The electronics naturally introduce a delay to the applied position-dependent electric forces, which could lead to deviations from the predictions of the perturbation theory discussed in Sec. II A. To qualitatively understand the effects of a delayed feedback nonlinear force, we have exaggerated the electronic delay τ applying a cubic force of the form $G_{\rm fb}x^3(t-\tau)$ for $\tau = (2\pi/4\omega_0) = T/4$ and $\tau = 6\pi/4\omega_0 =$

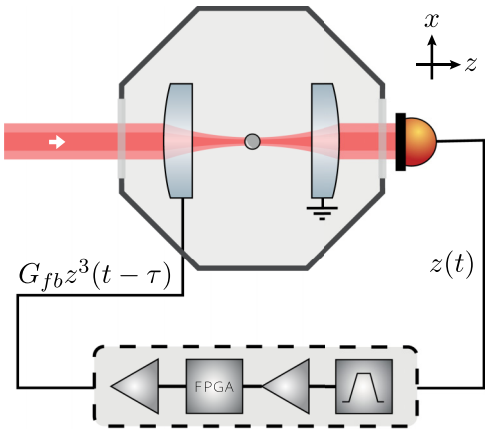

FIG. 1. Experimental setup. A silica nanoparticle is trapped by an optical tweezer in vacuum. The forward scattered light is collected and sent to a photodiode, producing a signal proportional to the particle's axial coordinate, $z(t)$. An FPGA processes the signal to produce a voltage that induces a force on the trapped particle proportional to $z^3(t-\tau)$. Amplification prior to and after the FPGA enhances the maximum resolution of its analog-to-digital converter, enabling the exploration of a broader range of values for the applied electrical force. The x direction pictured in the scheme is parallel to the optical table.

$3T/4$, and subsequently measured the PSDs of the particle motion along the longitudinal direction. The results can be seen in Fig. 2(a), in comparison to the PSD of the trapped particle in the absence of nonlinear feedback. We see that depending on the delay, the particle undergoes cooling ($\tau = T/4$) or heating ($\tau = 3T/4$). This can be understood as the nonlinear analog of cold damping, where the delayed feedback signal acquires a force component proportional to the velocity [31–33].

We can quantify the effect of delay for the case of our experiment using the theory described in Sec. II B. To do that, we have simulated the particle dynamics under the influence of a delayed feedback cubic force for two different values of the feedback gain G_{fb} within the regime of perturbation theory. For each simulation, we extract the particle motion traces and compute the position variance, from which the effective temperature T_{eff} of the mechanical oscillator can be obtained. The results are plotted in Fig. 2(b) as a function of τ, in comparison to the theoretical prediction given by Eq. (20). The simulations confirm the qualitative cooling and heating results shown in Fig. 2 and are in good agreement with the perturbation theory with the inclusion of delay. Notably, for the electronic delay in our experiment, characterized to be $\tau = (0.518 \pm 0.074) \times 10^{-6}$ s, we verify that the expected cooling and heating effects due to a delayed nonlinear feedback provide a correction to the autocorrelation at the level of 1.10% and are buried within experimental uncertainties. With this analysis, we conclude that any effect associated to electronic delay in our experiment is negligible and the perturbation theory in the absence of delay can be used to model the effect of nonlinear perturbations.

We next proceed to verify the perturbation theory as described in Sec. II A (without delay, $\tau = 0$). We apply an effective quartic perturbation to the optical potential by acting on the trapped particle with a cubic force which was generated, as previously described, from the position measurement feedback. PSDs of particle motion under the influence of the cubic feedback force with positive and negative feedback gains can be seen in Fig. 3(a). These measurements qualitatively confirm the effect of the cubic force predicted by perturbation theory as a shift in the PSD central frequency. Note the shift depends on the sign of the feedback gain, in accordance to Eq. (13), indicating an effective hardening or softening of the optical trap due to the cubic actuation.

To quantitatively compare the frequency shifts with the predictions from perturbation theory, we acquired the longitudinal motion PSD for different values of feedback gain

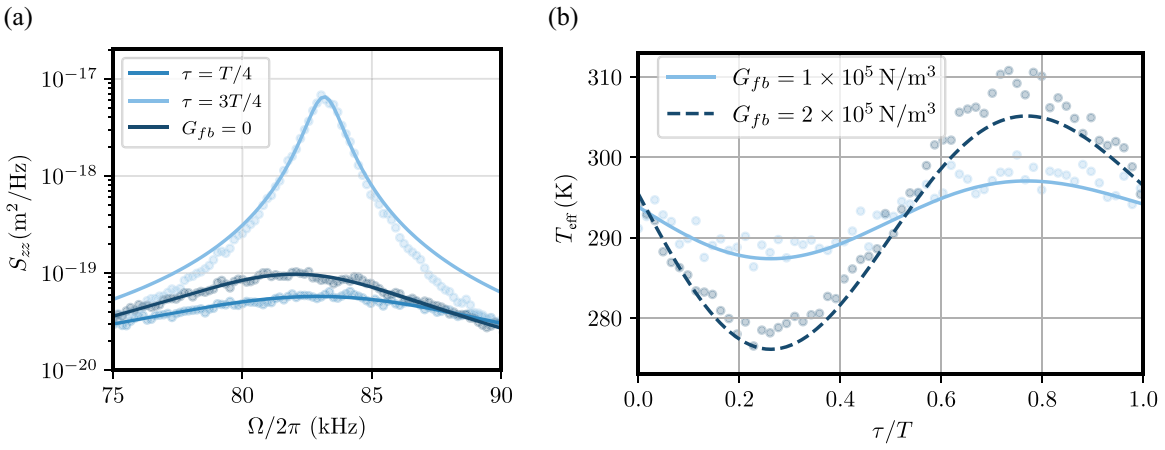

FIG. 2. Effect of a delayed nonlinearity. (a) Longitudinal position PSDs for the reference measurement (—) in comparison to cubic feedback forces at a gain of $G_{\mathrm{fb}} = 5.31 \times 10^6$ N/m^3 and delays of $\tau = T/4$ (—) and $\tau = 3T/4$ (—). Here, T represents the period of the particle motion along the longitudinal direction. These comparisons reveal how the introduction of a delayed cubic force can either cool or heat the particle motion. (b) Numerically simulated effective temperature T_{eff} of particle motion as a function of the delay in the cubic feedback force, displaying cooling and heating in accordance with the predictions of nonlinear delayed perturbation theory described in Sec. II B. With this analysis, we conclude that the electronic delay present in our experiment, measured to be $\tau/T = 0.042 \pm 0.006$, can be safely neglected.

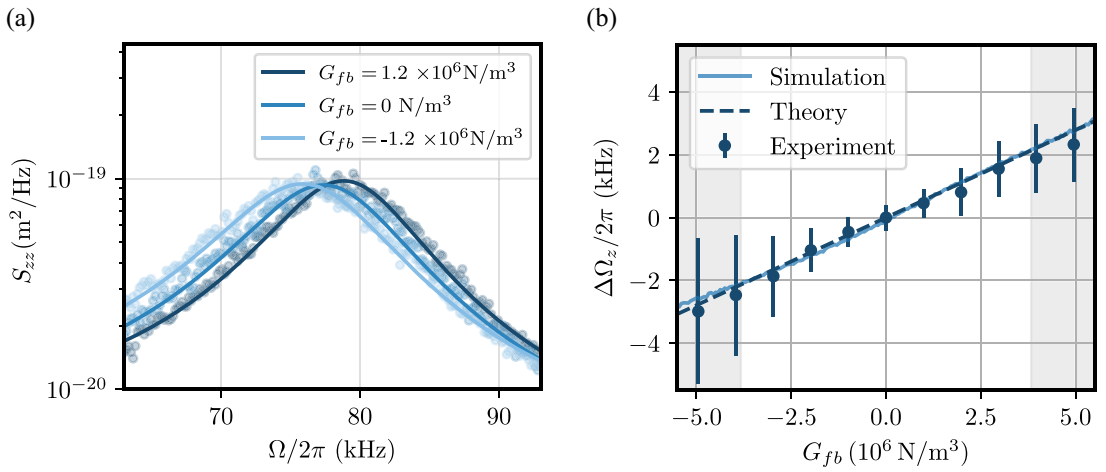

FIG. 3. Verifying the predictions of perturbation theory. (a) PSDs of the trapped particle's longitudinal motion under cubic force, displaying central frequency shifts. The data were taken at 293 K and a pressure of 10 mbar. The reference PSD (——) has a central frequency of 77.8 kHz and a shift of ±1.4 kHz was measured for $G_{\mathrm{fb}} = \pm 1.2 \times 10^6\ \mathrm{N/m^3}$. (b) Frequency shifts as a function of G_{fb}, verifying the prediction of perturbation theory given by Eq. (13) (dashed line). The gray-shaded region marks the regime of validity for perturbation theory described in Eq. (14). Each point corresponds to 250 seconds of data acquisition at 500 kHz divided into 1000 traces and organized into batches of 5 traces each. All data points were collected using the same nanoparticle.

G_{fb}. Note that all parameters going into κ [see Eq. (13)] are obtained from additional setup characterizations, leaving no free parameters to adjust the theory to the data. For instance, the trap central frequency ω_0 and mechanical damping Γ_m are obtained from Lorentzian fits of the unperturbed PSD, the nanoparticle mass m is calculated from the diameter provided by the manufacturer and from the density of silica, and the applied feedback gain G_{fb} is obtained after the calibration of the detector, electrode, and other intermediate electronic elements, as described in more detail in Appendix B. The particle is taken to be at ambient temperature $T_{\mathrm{eff}} = 293\,\mathrm{K}$; note that a 5 K variation in temperature yields a 2% variation in theoretical prediction.

Once these characterizations have been performed, the central frequencies of the perturbed PSDs—and, consequently, the associated shifts—can be obtained by a Lorentzian fit as a function of feedback gain and compared to the theoretical predictions. The result of these measurements is shown in Fig. 3(b), in comparison to the theoretical prediction given in Eq. (13) for our experimental parameters.

Good agreement between the data and the theoretical prediction was observed within the perturbation regime, indicated by the nonshaded region of the plot. Note, also, that outside the regime of perturbation theory [gray-shaded regions in Fig. 3(b)], the measured shifts systematically fall slightly below the predicted first-order correction, consistent with the second-order correction scaling of $O(G_{\mathrm{fb}}^2)$ [27]. Note that the error bars in Fig. 3(b) are larger for negative feedback in comparison to positive feedback gains. We attribute this to the fact that the intrinsic nonlinearity of the optical trap introduces an effective negative feedback gain ($G_{\mathrm{optical}} \approx 10^6\,\mathrm{N/m^3}$), shifting the regime of validity of perturbation to the right, towards positive gains [28]. Finally, the experimentally obtained angular coefficient κ_e was measured to be

$$\kappa_e = (5.46 \pm 0.10) \times 10^{-4}\ \mathrm{Hzm^3N^{-1}}, \tag{21}$$

which compares to the theoretical prediction given the parameters for our experiment,

$$\kappa_t = 5.69 \times 10^{-4}\ \mathrm{Hzm^3N^{-1}}. \tag{22}$$

IV. CONCLUSIONS

In conclusion, we have implemented a cubic nonlinear force based on position measurement feedback acting on an underdamped levitated nanoparticle. Effects of the cubic force on the particle's stochastic dynamics have been experimentally studied. In particular, shifts introduced in the particle motion power spectrum due to the presence of the cubic feedback force have been measured. We have verified that these shifts are in accordance with the predictions of the stochastic path-integral perturbation theory for nonlinear optical tweezers introduced in [27]. To account for the experimental imperfections due to electronic delay in the feedback, we have also extended the perturbation theory and showed that for feedback schemes currently available in levitated optomechanics experiments, the effects of electronic delay can be made negligible.

We anticipate that nonlinear electric feedback potentials will find a number of applications in levitated optomechanics experiments, both in the classical stochastic and quantum regimes. For instance, delayed nonlinear feedback can be used to engineer a nonconservative system with nonlinear damping of the van der Pol type [34]. Finally, weak measurements of a levitated optomechanical system in a cavity might allow for feedback-induced nonlinear dynamics in the quantum regime [35]—the nonclassical version of feedback-induced

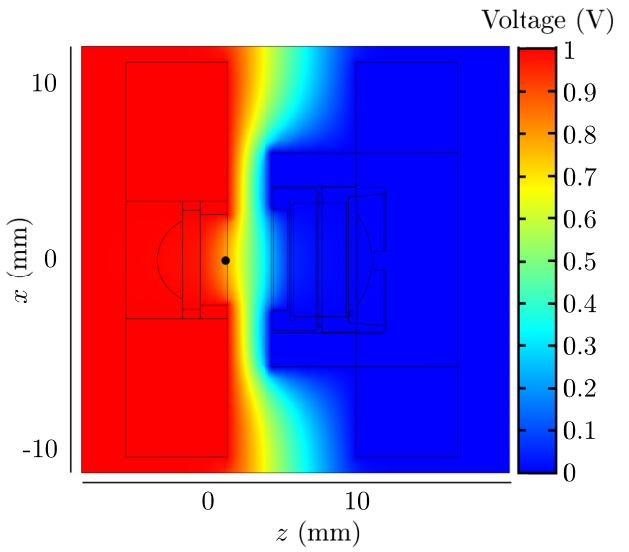

FIG. 4. Electric potential generated by the electrodes' geometry for a slice in the xz plane passing through the optical axis. The contour shows the internal structure of the optical setup, with the black dot marking the average position of the trapped particle, about 1.59 mm away from the flat base of the trapping lens.

nonlinear forces. In combination with recent advances in levitated quantum control experiments [33,36], weak nonlinear feedback could then enable the preparation of non-Gaussian states beyond the nonlinearities naturally present in optical potentials [16,37].

Code and data for this paper are available; see Ref. [38].

ACKNOWLEDGMENTS

We acknowledge B. Suassuna for helpful discussions. T.G. acknowledges the Coordenação de Aperfeiçoamento de Pessoal de Nível Superior - Brasil (CAPES) - Finance Code 001, Conselho Nacional de Desenvolvimento Científico e Tecnológico (CNPq), Fundação de Amparo à Pesquisa do Estado do Rio de Janeiro (FAPERJ Scholarship No. E-26/202.830/2019) and Fundação de Amparo à Pesquisa do Estado de São Paulo (FAPESP processo 2021/06736-5). D.T. acknowledges the Coordenação de Aperfeiçoamento de Pessoal de Nível Superior - Brasil (CAPES) - Finance Code 001, and Conselho Nacional de Desenvolvimento Científico e Tecnológico (CNPq) Scholarship No. 140197/2022-2.

APPENDIX A: ELECTRIC FIELD SIMULATION

One of the experiment's central assumptions is that the electric force acting upon the trapped particle is proportional to the voltage applied to the electrodes and does not depend on its position. Moreover, due to symmetry around the optical axis, we expect the components of the electric force orthogonal to the optical axis to be negligible. To verify these assumptions, a simulation of the electric potential and electric field generated by the geometry of the optical setup was conducted using COMSOL MULTIPHYSICS software (version 5.4).

In Fig. 4, the electrical potential between the electrodes is shown for a slice in the xz plane, where the internal contour of the optical setup is displayed for clarity. The left electrode, which contains the trapping lens, is set at 1 V relative to the right one, which holds the collection lens. The black dot denotes the average position of the trapped particle, 1.59 mm away from the flat base of the aspheric lens. Figures 5(a) and 5(b) show the electric field components in the vicinity of the particle. Considering an average amplitude of 100 nm for the COM motion, the simulation shows a percent change of roughly 0.01% for the z component of the electric field. Moreover, the x and y components are four to five orders of magnitude smaller than the z component, thus providing a firm foundation for our assumptions.

APPENDIX B: ELECTRONICS

In order to apply the feedback signal, essential steps were undertaken regarding the implementation of an electronic setup aimed at preprocessing the detection signal. First, it was crucial to address a strong DC component present in the signal obtained from the photodetector. To prevent saturation of the Red Pitaya RF input used in the experiment,

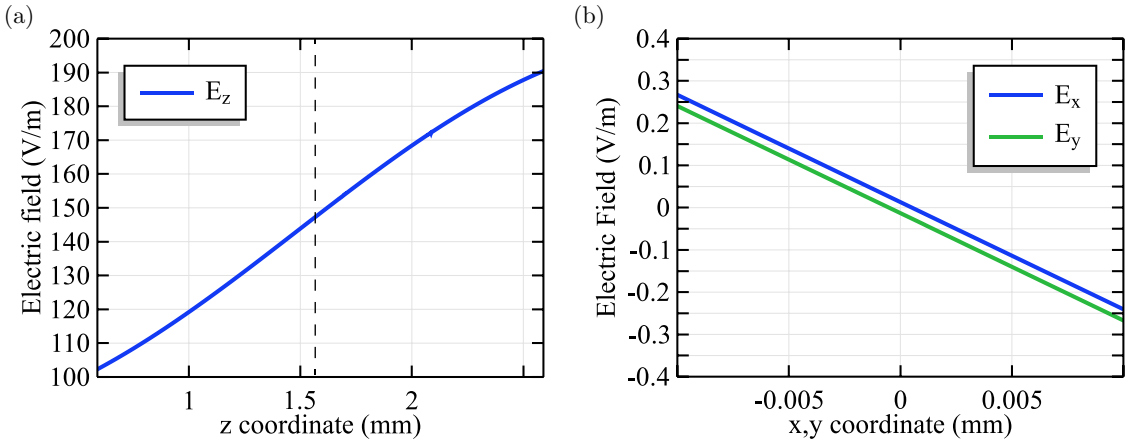

FIG. 5. The (a) z and (b) x, y components of the electric field in the vicinity of the trapped particle. The dashed line denotes the average position of the particle.

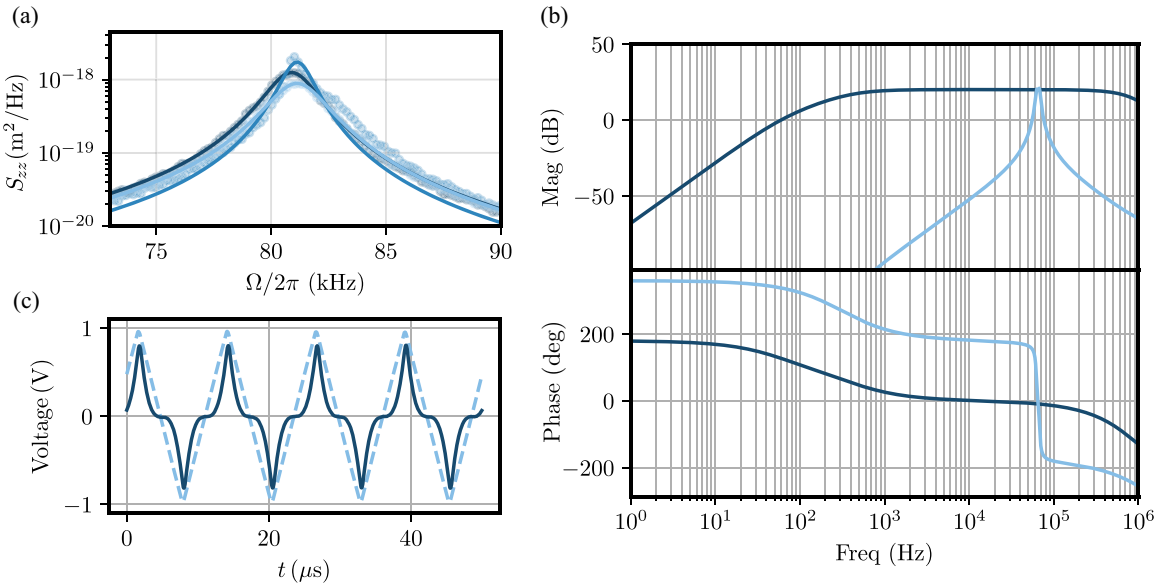

FIG. 6. Filter design. (a) PSDs obtained from simulations of a tweezed nanoparticle ($\Omega_z/2\pi = 81.5$ kHz and $\Gamma_m = 1.3 \times 10^4\,\mathrm{s}^{-1}$) under the influence of a cubic force. Three scenarios were considered: second-order Butterworth filter with 1 kHz bandwidth (——), 10 kHz bandwidth (——), and, lastly, with no filter (——). (b) Bode diagrams of a highly selective Butterworth filter (——) and of a passive RC filter (——); both circuits were simulated using LTspice XVII. (c) Results from the FPGA program. The dashed line represents the input, which is a triangular wave with a frequency of 81 kHz. The solid line corresponds to the output, which is proportional to the input raised to the third power.

an analog bandpass filter was implemented for its capability to effectively remove both DC and high-frequency components. While it is common to opt for a Butterworth filter based on the Sallen-Key topology [39], it is important to highlight that this choice introduces an undesirable phase effect.

As demonstrated by simulation results showed in Fig. 6(a), the addition of a Butterworth filter results in a shift of the PSD central frequency, which deviates from the theoretical prediction presented in [27]. To overcome this problem a passive RC filter is used along with a noninverter amplifier. As evident from Fig. 6(b), the comparison of the Bode diagrams for both topologies illustrates that the passive filter will have minimal impact on the signal phase, while simultaneously maintaining a flat band over a wider frequency range.

The addition of a noninverting amplifier after the bandpass filter enables the utilization of the full resolution of the analog-to-digital converter (ADC) on the Red Pitaya board. Furthermore, a second amplifier is incorporated after the FPGA, facilitating the generation of voltage values approximately 10 times higher than the board's limit. Upon characterization of both amplifiers, we found that the gains, A_1 and A_2, before and after the FPGA were measured as

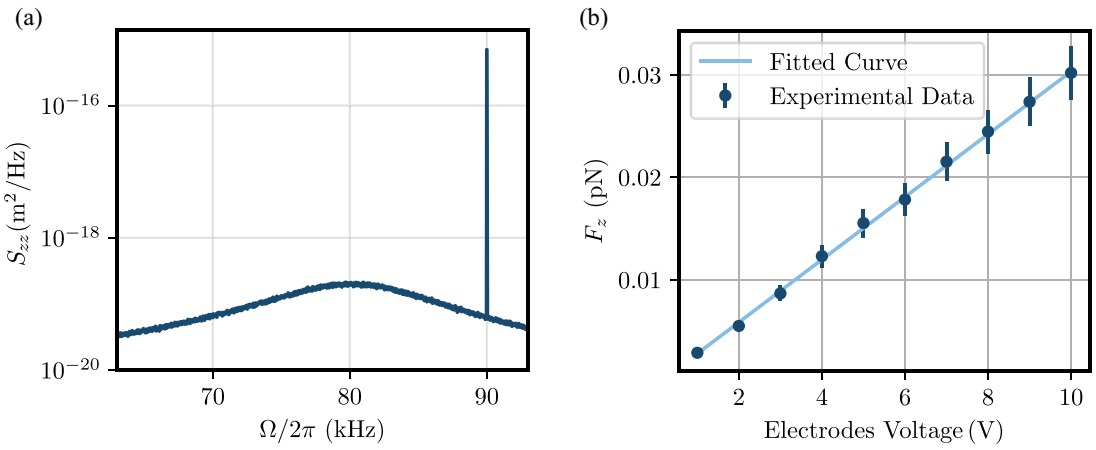

FIG. 7. Electrode calibration. (a) PSD obtained from a trapped nanoparticle at 10 mbar and $T_{\mathrm{eff}} = 293$ K under the action of a sinusoidal drive (voltage amplitude $V_0 = 10$ V and frequency $\omega_{dr}/2\pi = 90$ kHz). (b) Calibration curve for electrodes used to map the applied voltage to the resulting force applied on the nanoparticle.

11.00 V/V and 11.27 V/V, respectively. These values will be necessary for the calibration of the overall feedback gain $G_{\rm fb}$, detailed in Appendix C.

In Fig. 6(c), we illustrate an example of input and output signals of the Red Pitaya. In order to implement the nonlinear function, we employed fixed-point arithmetic—a method for representing fractional numbers within a specified range. This approach enables us to execute complex mathematical operations without suffering from information loss [40], as is often the case with binary representation. Furthermore, it offers a straightforward means to extend the code to implement higher-order polynomial functions.

APPENDIX C: CALIBRATION OF APPLIED FORCE

To validate the theoretical predictions outlined in [27], it was necessary to calibrate the overall feedback gain $G_{\rm fb}$, defined as

$$G_{\rm fb} = C_{NV} A_2 A_d A_1^3 C_{mV}^3, \tag{C1}$$

where A_1 and A_2 represent the gains originating from the electronic amplifiers, A_d is the tunable digital gain defined within the FPGA, C_{mV} is the calibration factor which converts the measured voltage into corresponding displacement in meters, and C_{NV} is the transduction coefficient that establishes the connection between the applied voltage across the electrodes and the resulting force applied to the particle; see Appendix B for further details.

To calibrate the photodetector, 1000 traces of 0.1 seconds were collected. The PSD of the time traces is fitted by a Lorentzian distribution,

$$S_{VV}(\omega) = \frac{D}{\Gamma_m^2 \omega^2 + \left(\omega^2 - \omega_0^2\right)^2}, \tag{C2}$$

where $D = 2\Gamma_m k_B T_{\rm eff} C_{mV}^2/m$; this takes into consideration that $S_{VV}(\omega) = C_{mV}^2 S_{zz}(\omega)$ [12]. This procedure led to a calibration factor of $C_{mV} = (1.504 \pm 0.073) \times 10^4$ V/m. After calibration of the detector, we proceed to determine the transduction coefficient, denoted as C_{NV}. To obtain C_{NV}, we subjected the particle to a series of sinusoidal signals with varying amplitudes and measured the particle's response in the position PSD [41]. For a particle subjected to Eq. (3), the total PSD $S_{zz}^T(\omega)$ in the presence of an electric drive, $F_{el}(t) = F_0 \cos(\omega_{dr} t)$, can be expressed as [41]

$$\begin{aligned} S_{zz}^T(\omega) &= S_{zz}(\omega) + S_{zz}^{el}(\omega) \\ &= \frac{2\Gamma_m k_B T_{\rm eff}}{m\left[\left(\omega^2 - \omega_0^2\right)^2 + \Gamma_m^2 \omega^2\right]} \\ &\quad + \frac{F_0^2 \tau_{el}\, \mathrm{sinc}^2[(\omega - \omega_{dr})\tau_{el}]}{m^2\left[\left(\omega^2 - \omega_0^2\right)^2 + \Gamma_m^2 \omega^2\right]}, \end{aligned} \tag{C3}$$

with τ_{el} being the duration of the measure. In Fig. 7(a), we display one of the PSDs used for the electrode calibration. The resulting calibration curve is presented in Fig. 7(b), which yields a transduction coefficient $C_{NV} = (3.06 \pm 0.13) \times 10^{-15}$ N/m. All measurements described in the main text were performed with the same nanoparticle.

[1] J. Millen, T. S. Monteiro, R. Pettit, and A. N. Vamivakas, Optomechanics with levitated particles, Rep. Prog. Phys. **83**, 026401 (2020).

[2] C. Gonzalez-Ballestero, M. Aspelmeyer, L. Novotny, R. Quidant, and O. Romero-Isart, Levitodynamics: Levitation and control of microscopic objects in vacuum, Science **374**, eabg3027 (2021).

[3] J. Gieseler and J. Millen, Levitated nanoparticles for microscopic thermodynamics—A review, Entropy **20**, 326 (2018).

[4] J. Gieseler, R. Quidant, C. Dellago, and L. Novotny, Dynamic relaxation of a levitated nanoparticle from a nonequilibrium steady state, Nat. Nanotechnol. **9**, 358 (2014).

[5] V. Svak, J. Flajšmanová, L. Chvátal, M. Šiler, A. Jonáš, J. Ježek, S. H. Simpson, P. Zemánek, and O. Brzobohatý, Stochastic dynamics of optically bound matter levitated in vacuum, Optica **8**, 220 (2021).

[6] J. Sheng, C. Yang, and H. Wu, Nonequilibrium thermodynamics in cavity optomechanics, Fundament. Res. **3**, 75 (2023).

[7] O. Romero-Isart, A. C. Pflanzer, F. Blaser, R. Kaltenbaek, N. Kiesel, M. Aspelmeyer, and J. I. Cirac, Large quantum superpositions and interference of massive nanometer-sized objects, Phys. Rev. Lett. **107**, 020405 (2011).

[8] G. Gasbarri, A. Belenchia, M. Carlesso, S. Donadi, A. Bassi, R. Kaltenbaek, M. Paternostro, and H. Ulbricht, Testing the foundation of quantum physics in space via interferometric and non-interferometric experiments with mesoscopic nanoparticles, Commun. Phys. **4**, 155 (2021).

[9] R. M. Pettit, W. Ge, P. Kumar, D. R. Luntz-Martin, J. T. Schultz, L. P. Neukirch, M. Bhattacharya, and A. N. Vamivakas, An optical tweezer phonon laser, Nat. Photon. **13**, 402 (2019).

[10] P. H. Jones, O. M. Maragò, and G. Volpe, *Optical Tweezers: Principles and Applications* (Cambridge University Press, Cambridge, 2015).

[11] J. Gieseler, J. R. Gomez-Solano, A. Magazzù, I. P. Castillo, L. P. García, M. Gironella-Torrent, X. Viader-Godoy, F. Ritort, G. Pesce, A. V. Arzola *et al.*, Optical tweezers—From calibration to applications: A tutorial, Adv. Opt. Photon. **13**, 74 (2021).

[12] E. Hebestreit, M. Frimmer, R. Reimann, C. Dellago, F. Ricci, and L. Novotny, Calibration and energy measurement of optically levitated nanoparticle sensors, Rev. Sci. Instrum. **89**, 033111 (2018).

[13] L. A. C. A. Defaveri, Silvio M. Duarte Queirós, and W. A. M. Morgado, Dependence of efficiency on the nonlinear nature of a nanomachine, Phys. Rev. E **98**, 062106 (2018).

[14] L. A. C. A. Defaveri, W. A. M. Morgado, and S. M. D. Queirós, Power output for a nonlinear Brownian machine, Phys. Rev. E **96**, 052115 (2017).

[15] F. Albarelli, A. Ferraro, M. Paternostro, and M. G. A. Paris, Nonlinearity as a resource for nonclassicality in anharmonic systems, Phys. Rev. A **93**, 032112 (2016).

[16] L. Neumeier, M. A. Ciampini, O. Romero-Isart, M. Aspelmeyer, and N. Kiesel, Fast quantum interference of a nanoparticle via optical potential control, Proc. Natl. Acad. Sci. USA **121**, e2306953121 (2024).

[17] Y. Yang, Y.-X. Ren, M. Chen, Y. Arita, and C. Rosales-Guzmán, Optical trapping with structured light: A review, Adv. Photon. **3**, 034001 (2021).

[18] L. Rondin, J. Gieseler, F. Ricci, R. Quidant, C. Dellago, and L. Novotny, Direct measurement of Kramers turnover with a levitated nanoparticle, Nat. Nanotechnol. **12**, 1130 (2017).

[19] F. Ricci, R. A. Rica, M. Spasenović, J. Gieseler, L. Rondin, L. Novotny, and R. Quidant, Optically levitated nanoparticle as a model system for stochastic bistable dynamics, Nat. Commun. **8**, 15141 (2017).

[20] Y. Zhang, J. Shen, C. Min, Y. Jin, Y. Jiang, J. Liu, S. Zhu, Y. Sheng, A. V. Zayats, and X. Yuan, Nonlinearity-induced multiplexed optical trapping and manipulation with femtosecond vector beams, Nano Lett. **18**, 5538 (2018).

[21] M. A. Ciampini, T. Wenzl, M. Konopik, E. Lutz, G. Thalhammer, M. Ritsch-Marte, M. Aspelmeyer, and N. Kiesel, Non-equilibrium memories with levitated nanoparticles: experimental verification of the generalised Landauer's principle, in *Optical Trapping and Optical Micromanipulation XVII*, Vol. 11463 (SPIE, 2020), p. 114631N.

[22] B. P. da Silva, V. A. Pinillos, D. S. Tasca, L. E. Oxman, and A. Z. Khoury, Pattern revivals from fractional Gouy phases in structured light, Phys. Rev. Lett. **124**, 033902 (2020).

[23] H. Moradi, V. Shahabadi, E. Madadi, E. Karimi, and F. Hajizadeh, Efficient optical trapping with cylindrical vector beams, Opt. Express **27**, 7266 (2019).

[24] B. Melo, I. Brandao, B. P. da Silva, R. B. Rodrigues, A. Z. Khoury, and T. Guerreiro, Optical trapping in a dark focus, Phys. Rev. Appl. **14**, 034069 (2020).

[25] F. Almeida, I. Sousa, O. Kremer, B. P. da Silva, D. Tasca, A. Khoury, G. Temporão, and T. Guerreiro, Trapping microparticles in a structured dark focus, Phys. Rev. Lett. **131**, 163601 (2023).

[26] C. C. Chow and M. A. Buice, Path integral methods for stochastic differential equations, J. Math. Neurosc. **5**, 8 (2015).

[27] B. Suassuna, B. Melo, and T. Guerreiro, Path integrals and nonlinear optical tweezers, Phys. Rev. A **103**, 013110 (2021).

[28] J. Gieseler, L. Novotny, and R. Quidant, Thermal nonlinearities in a nanomechanical oscillator, Nat. Phys. **9**, 806 (2013).

[29] M. T. Cuairan, J. Gieseler, N. Meyer, and R. Quidant, Precision calibration of the duffing oscillator with phase control, Phys. Rev. Lett. **128**, 213601 (2022).

[30] M. Innerbichler, A. Militaru, M. Frimmer, L. Novotny, and C. Dellago, White-noise fluctuation theorem for Langevin dynamics, New J. Phys. **24**, 113028 (2022).

[31] F. Tebbenjohanns, M. Frimmer, A. Militaru, V. Jain, and L. Novotny, Cold damping of an optically levitated nanoparticle to microkelvin temperatures, Phys. Rev. Lett. **122**, 223601 (2019).

[32] G. P. Conangla, F. Ricci, M. T. Cuairan, A. W. Schell, N. Meyer, and R. Quidant, Optimal feedback cooling of a charged levitated nanoparticle with adaptive control, Phys. Rev. Lett. **122**, 223602 (2019).

[33] F. Tebbenjohanns, M. L. Mattana, M. Rossi, M. Frimmer, and L. Novotny, Quantum control of a nanoparticle optically levitated in cryogenic free space, Nature (London) **595**, 378 (2021).

[34] N. P. Bullier, A. Pontin, and P. F. Barker, Quadratic optomechanical cooling of a cavity-levitated nanosphere, Phys. Rev. Res. **3**, L032022 (2021).

[35] S. Lloyd and Jean-Jacques E. Slotine, Quantum feedback with weak measurements, Phys. Rev. A **62**, 012307 (2000).

[36] L. Magrini, P. Rosenzweig, C. Bach, A. Deutschmann-Olek, S. G. Hofer, S. Hong, N. Kiesel, A. Kugi, and M. Aspelmeyer, Real-time optimal quantum control of mechanical motion at room temperature, Nature (London) **595**, 373 (2021).

[37] J. Bateman, S. Nimmrichter, K. Hornberger, and H. Ulbricht, Near-field interferometry of a free-falling nanoparticle from a pointlike source, Nat. Commun. **5**, 4788 (2014).

[38] O. Kremer, D. Tandeitnik, I. Califrer, and T. Guerreiro (2024), DOI: 10.5281/zenodo.10636075.

[39] R. Schaumann, H. Xiao, and V. V. Mac, *Design of Analog Filters*, 2nd ed. (Oxford University Press, Oxford, 2009).

[40] P. Wilson, *Design Recipes for FPGAs* (Newnes, London, UK, 2015).

[41] F. Ricci, M. T. Cuairan, G. P. Conangla, A. W. Schell, and R. Quidant, Accurate mass measurement of a levitated nanomechanical resonator for precision force-sensing, Nano Lett. **19**, 6711 (2019).